Thermal Effects of the Active Denial System

Hong Zhou

Department of Applied Mathematics
Naval Postgraduate School
Monterey, CA

Hongyun Wang

Department of Applied Mathematics
University of California
Santa Cruz, CA

Wesley A. Burgei

U.S. Department of Defense
Joint Non-Lethal Weapons Directorate
Quantico, VA

Abstract The Active Denial System (ADS) is a directed-energy, long-range, non-lethal weapon which sends a focused invisible beam of electromagnetic millimeter waves to the targets. Once the high-powered beam hits the target, the electromagnetic energy is absorbed in the skin and rapidly increases the skin temperature. High temperature activates the heat-sensitive nociceptors. When the stimulus is sufficiently strong, the withdrawal reflex is triggered and the subject pulls away from the beam. In this paper we study mathematically the heat-induced withdrawal reflex resulted from an exposure to millimeter waves. We developed a concise model to derive theoretical behaviors such as the time of reflex, biological latency of reflex, and the energy consumption by the time of reflex.

Keywords: Millimeter waves, Active Denial System, non-lethal weapon, nociceptors, heat-induced withdrawal reflex

1. Introduction

The Active Denial System (ADS) is a counter-personnel, low risk, non-lethal, directed-energy weapon that operates at the 95 GHz frequency with a corresponding wavelength of about 3.16 mm (or 0.12 inch) at a range up to 1000 meters. The ADS functions by directing a focused invisible man-sized (1.5m) beam of electromagnetic millimeter waves (MMWs) to the human targets from both mobile platforms and fixed sites [1]. The interaction of the electromagnetic fields with the human body depends on frequency, electromagnetic field strength and power,

type of exposure (continuous wave or pulsed) and duration. At 95GHz, the absorbed power is superficial with a penetration depth around 0.4mm. When the high-powered beam reaches the targeted individual, it rapidly causes an intolerable heating sensation that compels the target to move away from the beam. Once the target leaves the beam, the pain sensation vanishes instantly [2-3].

ADS is designed to support a full spectrum of operations including crowd control, riot dispersal, port protection, and area denial. Studies on human effects related to exposure to radio-frequency waves can be found in [4-8]. Some of the current research for ADS focus on reduction of cost, weight, size and risks.

Recently researchers at the Institute for Defense Analyses developed ADT CHEETEH-E model where ADT CHEETEH-E stands for Active Denial Technology Computational Human Effects End-To-End Hyper-model for Effectiveness [9]. In this model, the process from the power emitted at the radiation antenna to the subject's behavioral response is separated into several steps and each step is described by its own model components which contain specific function forms and parameters. In this study, we follow the ADT CHEETEH-E model as general guidelines and construct a concise dose-response relation for predicting the occurrence of withdrawal reflex based on spatial temperature profiles. Our concise model does not depend on the specific function forms or parameters used in the ADT CHEETEH-E model. In contrast, our dose-response model is specified by only two parameters: the activation temperature of nociceptors (T_{act}) and the critical threshold on the dose quantity (z_c). We define the dose quantity as the volume of activated region where the temperature is above the activation temperature of nociceptors. When the spatial temperature profile at reflex is measurable, the two model parameters T_{act} and z_c can be determined from the test data.

2. A Concise Model for the Withdrawal Reflex

Our main concern is the occurrence of withdrawal reflex, observed as a target moving out of beam. We follow the model components proposed in [9] as guidelines. We adopt the same assumption that the perceived pain level at time *t* is solely determined by the number of activated nociceptors at time *t*, which in turn is entirely determined by the temperature profile at time *t*. Our goal is to construct a concise model that is broadly applicable and contains only a few parameters. First, we introduce a few notations.

- $T(\boldsymbol{r}, y, t)$: temperature at depth *y* below the skin surface at time *t*

- T_{act} : the activation temperature of heat-sensitive nociceptors

Given spatial temperature profile $T(\boldsymbol{r}, y)$, our objective is to predict the corresponding binary outcome with respect to the outcome of withdrawal reflex. For this purpose, we choose the activated volume as the dose quantity:

$$z \equiv z\left(\{T\}, T_{\text{act}}\right) = \int I_{(T \geq T_{\text{act}})} d\boldsymbol{r} dy. \tag{1}$$

where we use $\{T\}$ as a concise notation for the spatial temperature profile $T(\boldsymbol{r}, y)$ and the indicator function $I_{(T \geq T_{\text{act}})}$ takes the form of the Heaviside step function:

$$I_{(T \geq T_{\text{act}})}(\boldsymbol{r}, y, t) = \begin{cases} 0, \text{ if } T(r, y, t) < T_{act} \\ 1, \text{ if } T(r, y, t) \geq T_{act}. \end{cases} \tag{2}$$

The deterministic dose-response model is given by the unit step function:

$$\text{outcome}(z) = \begin{cases} 0 \ (\text{no withdrawal reflex}), & \text{if } z < z_c \\ 1 \ (\text{withdrawal reflex occurs}), & \text{if } z \geq z_c, \end{cases} \tag{3}$$

where z_c is the dose threshold for the withdrawal reflex to happen. It is worthwhile to note that our model is completely specified by two parameters T_{act} and z_c even though the dose threshold z_c depends on many internal hidden parameters such as the perceived pain level, the density of heat-sensitive nociceptors in the subject's skin, and motivation-modulated perceived pain level. Once the values of T_{act} and z_c are known, the above dose-response model is completely defined.

3. Determination of the Two Model Parameters from Test Data

Now we provide a methodology of using test data to derive the two parameters in our concise model, namely, the activation temperature T_{act} and the dose threshold z_c. We focus on the hypothetical situation where the temperature of the skin as a function of the 3-D spatial coordinates and time is measurable in experiments. Since our dose-response model (3) appeals to the assumption that the occurrence of withdrawal reflex at time t_{ref} is only attributed to the spatial temperature profile at t_{ref}, it follows that only $T(\boldsymbol{r}, y, t_{\text{ref}})$ is relevant for determining the two model parameters T_{act} and z_c. Given $T(\boldsymbol{r}, y, t_{\text{ref}})$, we can set the activation temperature T_{act} to any reasonable value within the range of $T(\boldsymbol{r}, y, t_{\text{ref}})$.

Then, for each value of T_{act}, the associated dose threshold z_c is the activated volume, calculated from $T(\boldsymbol{r}, y, t_{\text{ref}})$ according to the selected activation temperature. More precisely,

$$z_c = \text{volume of } \left\{(\boldsymbol{r}, y) \middle| T(\boldsymbol{r}, y, t_{\text{ref}}) \geq T_{\text{act}} \right\} \equiv z_c(T_{\text{act}}). \tag{4}$$

Note that function $z_c(T_{\text{act}})$ defined in (4) decreases monotonically with T_{act}. However, one temperature profile $T(\boldsymbol{r}, y, t_{\text{ref}})$ does not provide enough information for determining both T_{act} and z_c simultaneously. In a deterministic model, at a given set of test condition $(P_{\text{dep}}(\boldsymbol{r}), A)$ where $P_{\text{dep}}(\boldsymbol{r})$ is the power density deposited on the skin surface and *A* is the beam spot area, the time of withdrawal reflex t_{ref} and the temperature profile at reflex $T(\boldsymbol{r}, y, t_{\text{ref}})$ are both fixed. Hence at a given set of test conditions, the measurements give only one constraint function $z_c(T_{\text{act}})$ on the two unknown parameters. When the test condition $(P_{\text{dep}}(\boldsymbol{r}), A)$ varies experimentally, the reflex time t_{ref} and the temperature profile at reflex $T(\boldsymbol{r}, y, t_{\text{ref}})$ will change, and consequently, the constraint function $z_c(T_{\text{act}})$ will differ. The influence of test condition on the constraint function shines lights on building substantially distinct equations for (T_{act}, z_c) from data measured at different test conditions. Once we obtain two different constraint equations for the pair (T_{act}, z_c), these two unknown parameters can be found by solving a 2x2 system:

$$\begin{aligned} z_c - z_c(T_{\text{act}})\big|_{(\text{test condition 1})} &= 0 \\ z_c - z_c(T_{\text{act}})\big|_{(\text{test condition 2})} &= 0. \end{aligned} \tag{5}$$

As an example, Figure 1 illustrates constraint functions constructed with simulated test data in the case without heat conduction with two different beam spot areas: $\frac{A}{\mu} = 1$ and $\frac{A}{\mu} = 4$. As shown in Figure 1, when the constraint functions obtained from two tests are

significantly distinct from each other, the well-defined intersection of the two curves yields the true values of (T_{act}, z_c), denoted as $(T_{\text{act}}^*, z_c^*)$.

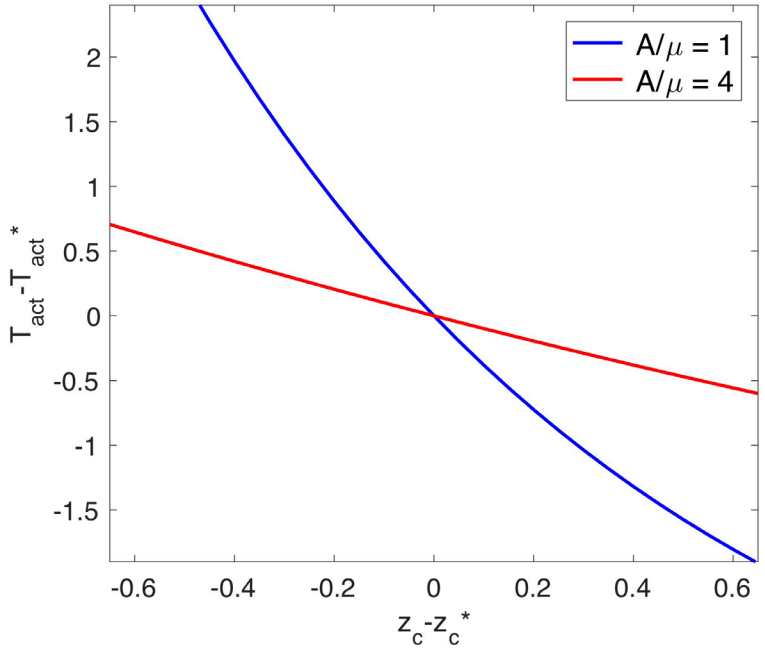

Figure 1. Constraint functions on (T_{act}, z_c) for an idealized case without heat conduction. The steepness of $T_{\text{act}}(z_c)$ varies with $\frac{A}{\mu}$. The intersection of the two distinct constraint functions determines the true value of (T_{act}, z_c), labeled as $(T_{\text{act}}^*, z_c^*)$.

4. Non-dimensionalization and Heat Conduction in the Skin Depth Direction

We investigate the effect of heat conduction along the *y*-direction (the depth direction of the skin). We restrict our attention to the following scenario.

- At any given time, the temperature is uniform over the beam cross-section *A* (i.e. independent of ***r***) and is a decreasing function of skin depth *y*.
- Outside the beam cross-section, the temperature is always below the activation temperature (for example, at the normal body temperature).
- The effect of heat conduction occurs in the skin depth direction with uniform thermal conductivity.

The temperature distribution is specified by the heat conduction along the skin depth direction with electromagnetic heating caused by electromagnetic energy absorbed:

$$\rho c_p \frac{\partial T(\mathbf{r},y,t)}{\partial t} = k \frac{\partial^2 T(\mathbf{r},y,t)}{\partial y^2} + p_{\text{dep}} \mu e^{-\mu y} \quad \text{for } \mathbf{r} \in A$$
$$\left. \frac{\partial T(\mathbf{r},y,t)}{\partial y} \right|_{y=0} = 0 \qquad T(\mathbf{r},y,0) = T_0. \tag{6}$$

Here $\rho, c_p,$ and k denote the mass density, specific heat capacity, and thermal conductivity of the subject's skin, respectively, p_{dep} defines the power density deposited on the skin surface, $1/\mu$ describes the characteristic depth that the millimeter wave penetrates into the skin, and T_0 is the initial temperature. In the initial boundary value problem (6), an insulated boundary condition is imposed at the skin surface $(y = 0)$.

To facilitate our analysis, we introduce a temperature scale ΔT, the characteristic difference between the initial temperature T_0 and the nociceptor activation temperature T_{act}, together with a length scale $y_s \equiv \frac{1}{\mu}$ and a time scale $t_s \equiv \frac{\rho c_p}{k\mu^2}$. We use these characteristic scales to carry out non-dimensionalization and arrive at

$$\frac{\partial T_{\text{nd}}}{\partial t_{\text{nd}}} = \frac{\partial^2 T_{\text{nd}}}{\partial y_{\text{nd}}^{\ 2}} + p_{\text{dep,nd}} e^{-y_{\text{nd}}}$$
$$\left. \frac{\partial T_{\text{nd}}}{\partial y_{\text{nd}}} \right|_{y_{\text{nd}}=0} = 0 \qquad T(y_{\text{nd}},0) = 0, \tag{7}$$

where the dimensionless variables and parameters are

$$y_{\text{nd}} = \frac{y}{y_s} = \mu y, \quad t_{\text{nd}} = \frac{t}{t_s} = \frac{k\mu^2}{\rho c_p} t, \quad T_{\text{nd}} = \frac{T - T_0}{\Delta T}, \quad \text{and} \quad p_{\text{dep,nd}} = \frac{p_{\text{dep}}}{k\mu\Delta T}.$$

After some mathematical manipulations, we derive the analytical solution for the non-dimensional temperature distribution:

$$T_{\text{nd}}(y_{\text{nd}},t_{\text{nd}}) = P_{\text{dep,nd}} H(y_{\text{nd}},t_{\text{nd}})$$
$$H(y,t) = \int_0^t G(y,s)\,ds \tag{8}$$
$$G(y,t) = \frac{1}{2}\operatorname{erfc}\left(\frac{2t-y}{\sqrt{4t}}\right)e^{t-y} + \frac{1}{2}\operatorname{erfc}\left(\frac{2t+y}{\sqrt{4t}}\right)e^{t+y},$$

where the complementary error function is written as

$$\operatorname{erfc}(x)=\frac{2}{\sqrt{\pi}}\int_{x}^{\infty}\exp\left(-s^{2}\right)ds. \tag{9}$$

The pre-scaling physical temperature distribution $T(y,t)$ is

$$T(y,t)-T_0=\Delta T\cdot P_{\text{dep,np}}H\left(\frac{y}{y_s},\frac{t}{t_s}\right)=\frac{P_{\text{dep}}}{k\mu}H\left(\mu y,t\frac{k\mu^2}{\rho c_p}\right). \tag{10}$$

Equation (10) expresses the physical temperature distribution $T(y,t)$ as a scaling and shifting of $H(y,t)$. The normalized non-dimensional temperature $H(y,t)$ is a standardized parameter-free function. While the shifting depends on the initial temperature, the scaling relies on parameters of electromagnetic wave, energy absorption and heat conduction.

5. Effect of Heat Conduction

To assess the effect of heat conduction, we compare the solution without heat conduction $H_0(y,t)$ with the one with heat conduction $H(y,t)$ in Figure 2, together with the relative error $Err(y,t)=\dfrac{H_0(y,t)-H(y,t)}{H(y,t)}$ in Figure 3. In these two figures *y* and *t* are the dimensionless depth and time. In the lightly-shaded rectangular region in Figure 3 where $t_{\text{nd}}\le 0.102$ and $y_{\text{nd}}\ge 0.258$, the absolute value of the relative error in the no-conduction approximation is less than 5%. No-conduction approximation is valid only at a depth away from the skin surface. When the skin depth is small, one needs to restrict the time to a very small range in order to retain a reasonably low relative error. For instance, at depth $y_{\text{nd}}=0.05$, to make the relative error below 5%, one has to limit the dimensionless time to the tiny interval of $t_{\text{nd}}\le 0.015$ (darkly-shaded rectangle in Figure 3).

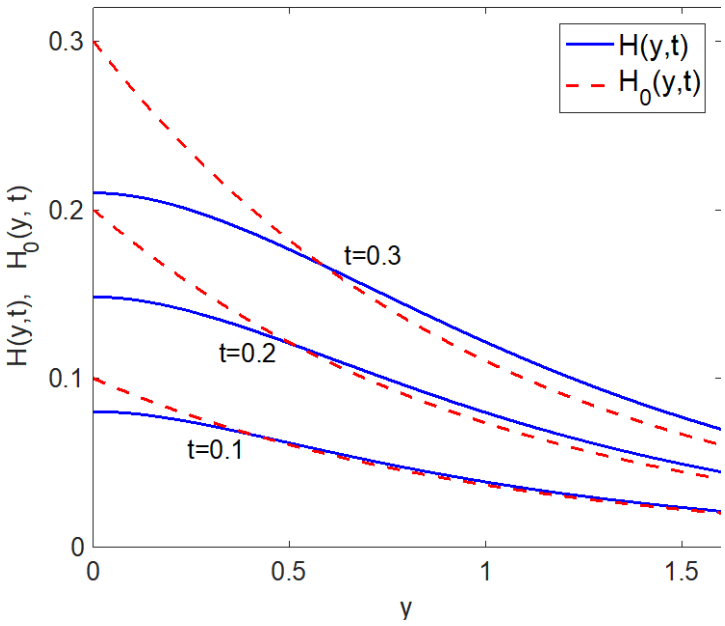

Figure 2. Comparison of solutions $H_0(y,t)$ (without) and $H(y,t)$ (with heat conduction).

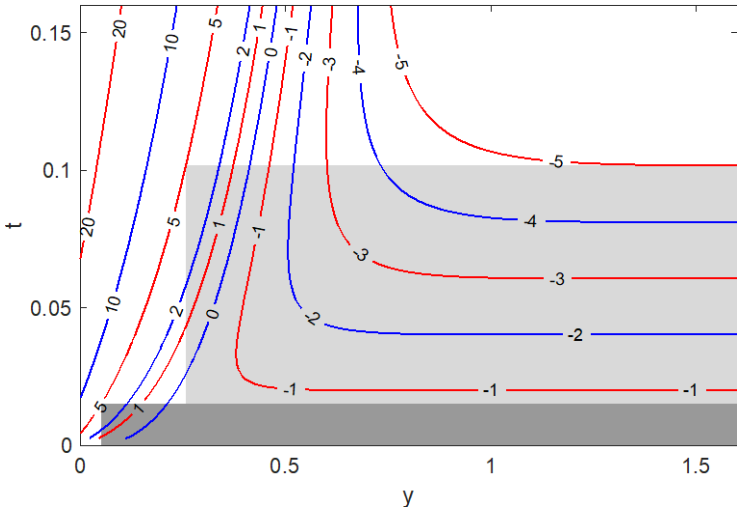

Figure 3. Contour lines of relative error $Err(y,t)$ in percentage. For example, the contour line labeled with (-1) represents a relative error of (-1%).

6. Theoretical Behaviors of the System

We examine the reflex time vs. beam spot area, the biological latency in withdrawal reflex, asymptotics of the normalized temperature for small *t* and for large *t*, the energy consumption at small and at large applied power density, the spatial temperature profile at reflex, and constraints

on model parameters constructed from temperature profiles. We list our main results as follows, skipping all the mathematical details. Complete derivations can be found in [10].

Reflex time vs. beam spot area: The physical reflex time with heat conduction takes the form

$$t_{\text{ref}}(A)=\frac{\rho c_p}{k\mu^2}t_0\left[1+c_A\left(\frac{\mu z_c}{A}\right)^2+\cdots\right], \tag{11}$$

where t_0 and c_A are given by

$$t_0=h^{-1}\left(\frac{(T_{\text{act}}-T_0)K\mu}{P_{\text{dep}}}\right),\quad c_A=\frac{1-\text{erfc}\left(\sqrt{t_0}\right)e^{t_0}}{2\text{erfc}\left(\sqrt{t_0}\right)e^{t_0}t_0}, \tag{12}$$

and $h^{-1}(\cdot)$ denotes the inverse function of $h(t)$ defined by

$$h(t)=\text{erfc}\left(\sqrt{t}\right)e^t-1+\frac{2}{\sqrt{\pi}}\sqrt{t}. \tag{13}$$

It can be shown that the asymptotic behaviors of $h(t)$ and $h^{-1}(u)$ satisfy

$$\begin{aligned} h(t)&=t\left(1-\frac{4}{3\sqrt{\pi}}\sqrt{t}+\frac{t}{2}+\cdots\right) \quad \text{for small } t\\ h(t)&=\frac{2\sqrt{t}}{\sqrt{\pi}}\left(1-\frac{\sqrt{\pi}}{2\sqrt{t}}+\frac{1}{2t}+\cdots\right) \quad \text{for large } t \end{aligned} \tag{14}$$

and

$$\begin{aligned} h^{-1}(u)&=u+\frac{4}{3\sqrt{\pi}}u^{3/2}+\left(\frac{8}{3\pi}-\frac{1}{2}\right)u^2+\cdots \quad \text{for small } u\\ h^{-1}(u)&=\frac{\pi}{4}\left[u^2+2u+\left(1-\frac{4}{\pi}\right)+\cdots\right] \quad \text{for large } u. \end{aligned} \tag{15}$$

It is easy to see from formula (11) that as the beam spot area A increases, the reflex time converges rapidly to a positive value above zero.

Biological latency in withdrawal reflex: The time delay is the time between the moment when enough nociceptors are activated to initiate the withdrawal reflex and the moment when the actual reflex action occurs in the observation. In experiments, both applied power density P_{dep} and the beam spot area A can be tuned. While the reflex

time varies with P_{dep} and A, we assume that the time delay in observed reflex is an intrinsic biological property of the test subject and is independent of P_{dep} and A. Thus, the observed reflect time is the sum of the true reflex time and the unknown time delay: $t_{\text{obs}} = t_{\text{ref}} + t_{\text{del}}$ where the true reflex time t_{ref} is described as a function of P_{dep} and A in equations (11) and (12). We design a strategy to determine the time delay t_{del} using the observed reflex times at a sequence of P_{dep} values. More specifically, we make observations at three different values of P_{dep}: $P_{\text{dep}} = p_0$, $P_{\text{dep}} = 2p_0$, and $P_{\text{dep}} = 4p_0$. We proceed by introducing an auxiliary quantity

$$v_{\text{obs}} = \frac{\left[t_{\text{obs}}(p_0) - t_{\text{obs}}(2p_0)\right] - 2\left[t_{\text{obs}}(2p_0) - t_{\text{obs}}(4p_0)\right]}{\left[t_{\text{obs}}(p_0) - t_{\text{obs}}(2p_0)\right] + 2\left[t_{\text{obs}}(2p_0) - t_{\text{obs}}(4p_0)\right]} \tag{16}$$

and a monotonically increasing function

$$R(u) = \frac{\left[h^{-1}(u) - h^{-1}\left(\frac{u}{2}\right)\right] - 2\left[h^{-1}\left(\frac{u}{2}\right) - h^{-1}\left(\frac{u}{4}\right)\right]}{\left[h^{-1}(u) - h^{-1}\left(\frac{u}{2}\right)\right] + 2\left[h^{-1}\left(\frac{u}{2}\right) - h^{-1}\left(\frac{u}{4}\right)\right]}, \tag{17}$$

where function $h(t)$ is embodied in the parameter-free expression (13). We further observe that

$$\begin{aligned} R(u) &= \frac{5-3\sqrt{2}}{3\sqrt{\pi}}u^{1/2} + \left(\frac{4\sqrt{2}}{9\pi} - \frac{3}{16}\right)u + \cdots \quad \text{for small } u \\ R(u) &= \frac{1}{3}\left[1 - \frac{16}{9u} + \frac{16^2}{9^2u^2} + \cdots\right] \quad \text{for large } u. \end{aligned} \tag{18}$$

Consequently, the time delay calculated from three data points may be written as

$$t_{\text{del}}^{(\text{est})} = t_{\text{obs}}(p_0) - c_1^{(\text{est})} h^{-1}\left(\frac{c_2^{(\text{est})}}{p_0}\right) \tag{19}$$

with corresponding coefficients

$$c_2^{(\text{est})} = p_0 R^{-1}(v_{\text{obs}}),\ c_1^{(\text{est})} = \frac{t_{\text{obs}}(p_0) - t_{\text{obs}}(2p_0)}{h^{-1}\left(\frac{c_2^{(\text{est})}}{p_0}\right) - h^{-1}\left(\frac{c_2^{(\text{est})}}{2p_0}\right)}. \tag{20}$$

Normalized temperature for small/large *t*: The normalized dimensionless temperature $H(y,t)$ at a fixed skin depth y has the following asymptotic formula:

$$H(y,t) = e^{-y}\left(e^{t}-1\right) + \text{T.S.T.} \quad \text{for small } t$$

and (21)

$$H(y,t) = \frac{2}{\sqrt{\pi}}t^{1/2} - \left(e^{-y}+y\right) + \frac{2+y^2}{2\sqrt{\pi}}t^{-1/2} + \cdots \quad \text{for large } t$$

where T.S.T. is the abbreviation for Transcendentally Small Terms, which converge to zero faster than any powers of t. Figure 4 depicts the scaled exact solution $H(y,t)/t$, its asymptotic approximations (21) for small t and large t, and the scaled no-conduction approximation at a fixed skin depth $y = 1$.

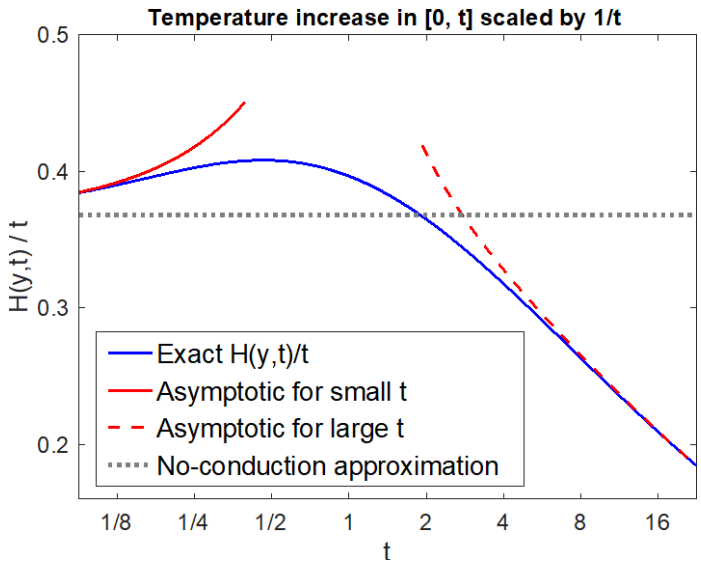

Figure 4. Scaled temperature profiles with asymptotic approximations.

Reflex times at small/large applied power densities: The dimensionless reflex time is highly influenced by the applied power density. For example, for small $P_{\text{dep,nd}}$ it has the complicated form,

$$t_{\mathrm{ref,nd}}\left(P_{\mathrm{dep,nd}}\right)=$$
$$\frac{\pi\left(T_{\mathrm{act,nd}}\right)^2}{4\left(P_{\mathrm{dep,nd}}\right)^2}\left[1+2\left(e^{-\frac{1}{A_{\mathrm{nd}}}}+\frac{1}{A_{\mathrm{nd}}}\right)+\frac{P_{\mathrm{dep,nd}}}{T_{\mathrm{act,nd}}}+\left(\left(e^{-\frac{1}{A_{\mathrm{nd}}}}+\frac{1}{A_{\mathrm{nd}}}\right)^2-\frac{2}{\pi}\left(2+\frac{1}{{A_{\mathrm{nd}}}^2}\right)\right)\frac{\left(P_{\mathrm{dep,nd}}\right)^2}{\left(T_{\mathrm{act,nd}}\right)^2}+\cdots\right] \quad (22)$$

and for large $P_{\mathrm{dep,nd}}$

$$t_{\mathrm{ref,nd}}\left(P_{\mathrm{dep,nd}}\right)=\ln\left(1+\frac{T_{\mathrm{act,nd}}}{P_{\mathrm{dep,nd}}}e^{\frac{1}{A_{\mathrm{nd}}}}\right). \quad (23)$$

In Figure 5 we plot the energy deposited per area on skin by the time of reflex $t_{\mathrm{dep,nd}}\left(P_{\mathrm{dep,nd}}\right)P_{\mathrm{dep,nd}}$, its asymptotic approximations (22) and (23), and the no-conduction approximation. Interestingly, the energy consumption has a minimum with respect to the applied power density. The minimum energy consumption is attained when $P_{\mathrm{dep,nd}}$ is moderately large, as shown in Figure 5.

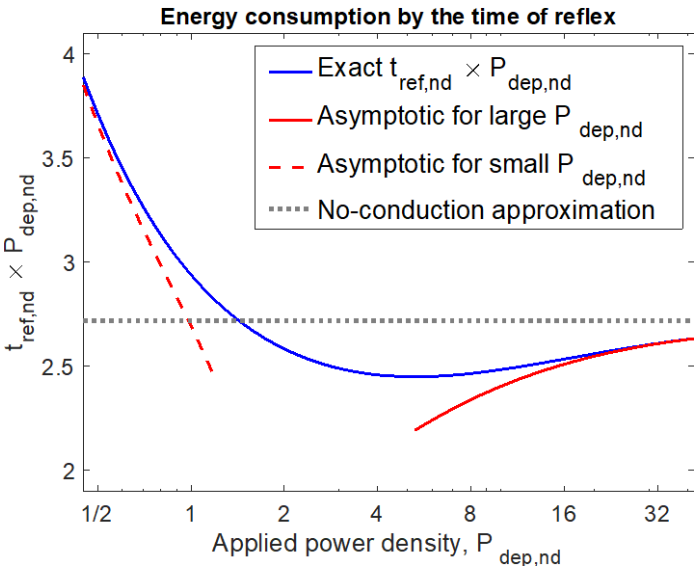

Figure 5. Energy consumption by the time of reflex for various solutions.

Spatial temperature profile at reflex: At reflex, the dimensionless temperature is determined by

$$T_{\mathrm{nd}}\left(y_{\mathrm{nd}}\right)\big|_{\mathrm{reflex}} = P_{\mathrm{dep,nd}} H\left(y_{\mathrm{nd}}, t_{\mathrm{ref,nd}}\right)$$

$t_{\mathrm{ref,nd}}$ is the solution of $H\left(\frac{1}{A_{\mathrm{nd}}}, t_{\mathrm{ref,nd}}\right) = \frac{T_{\mathrm{act,nd}}}{P_{\mathrm{dep,nd}}}$.

Figure 6 shows snapshots of the dimensionless temperature profile at reflex for different applied power densities. From Figure 6 it is apparent that at a fixed skin depth y, as $P_{\mathrm{dep,nd}}$ increases the temperature at reflex converges to the solution with no-heat conduction. Therefore, at any fixed skin depth away from the skin surface, the effect of heat conduction is eventually insignificant when the applied power density is large enough.

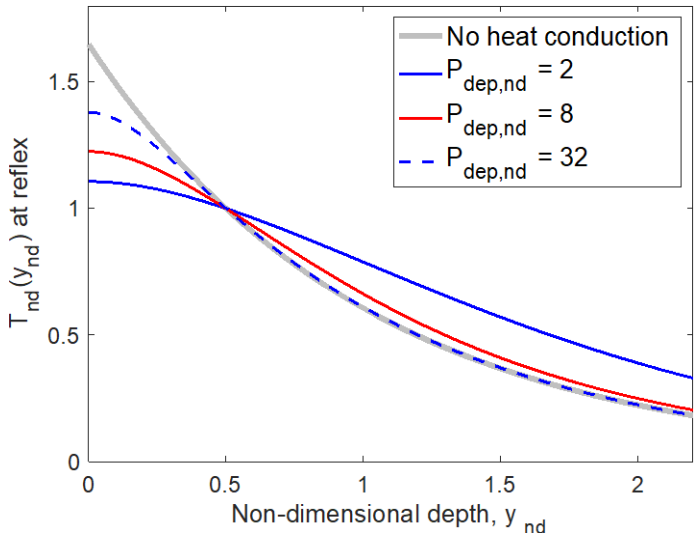

Figure 6. Dimensionless temperature profile at reflex for various values of applied power densities where $T_{\mathrm{act,nd}} = 1, A_{\mathrm{nd}} = 2$.

Finally, we remark that in order to reliably determine model parameters $\left(T_{\mathrm{act}}, z_c\right)$, one needs to carry out tests with significantly different sets of beam spot area.

7. Conclusions

We studied mathematically the occurrence of heat-induced withdrawal reflex caused by exposure to an electromagnetic beam such as ADS. We developed a concise two-parameter model for predicting the occurrence of withdrawal reflex based on the given spatial temperature profile. In the dose-response relation, the dose quantity is chosen as the volume of the activated region of heat-sensitive nociceptors. Under the assumption that the density of nociceptors in the

skin is uniform, the activated volume is proportional to the total number of nociceptors activated. Therefore, it grows monotonically as the perceived pain level goes up, which controls the occurrence of withdrawal reflex. In a deterministic setting, withdrawal reflex happens exactly when the activated volume reaches a critical threshold. Our model contains two parameters: the activation temperature of nociceptors and the critical threshold on the activated volume. We showed that these two parameters can be determined from test data where the reflex time and the spatial temperature profile of the skin at reflex are measurable. More specifically, we need to carry out tests with a moderate beam spot area and with a large beam spot area in order to accurately estimate the two model parameters. Furthermore, we analyzed the theoretical behaviors of the system and our main findings include:

- As the beam spot area increases, the reflex time decreases rapidly to a positive value above zero.
- The time delay between the observed reflex time and the true reflex time can be evaluated from measured values of the observed reflex time at a sequence of applied power densities. Once the time delay is found, the true reflex time effectively becomes measurable.
- The (true) reflex time decreases when the applied power density is increased.
- At a fixed skin depth, for large power density, the temperature at reflex converges to the solution without heat conduction. This result suggests that it is appropriate to ignore the effect the heat conduction only when the location is away from the skin surface and the dimensionless power density is large.

Acknowledgment and Disclaimer

The authors would like to acknowledge support of the Joint Non-Lethal Weapons Directorate of U.S. Department of Defense and the Naval Postgraduate School. The views expressed in this document are those of the authors and do not reflect the official policy or position of the Department of Defense or the U.S. Government.

References

1. https://jnlwp.defense.gov/About/Frequently-Asked-Questions/Active-Denial-System-FAQs/

2. J. Parker, D. Ryan, J. Moreno, W. Voorhees and J. Whitmore (2014) "Meta-analysis of thermal effects from 94Ghz, millimeter wave exposures on humans", AFRL report
3. J. Parker, C. Beason, W. Voorhees and J. Whitmore (2015) "Extension of meta-analysis of thermal effects from 94GHz, millimeter wave exposures on humans incorporating skin depth", AFRL report
4. T.J. Walters, D.W. Blick, L.R. Johnson, E.R. Adair, and K.R. Foster, “Heating and pain sensation produced in human skin by millimeter waves: comparison to a simple thermal model”, Health Phys., vol. 78, no. 3, pp. 259-267, Mar. 2000
5. S. Ozen, S. Helhel, and O. Cerezci, “Heat analysis of biological tissue exposed to microwave by using thermal wave model of bio-heat transfer (TWMBT)”, Burns, 34, 45-49, 2008
6. S. Ozen, S. Helhel, and S. Bilgin, “Temperature and burn injury prediction of human skin exposed to microwaves: a model analysis”, Radiat Environ Biophys, 50, 483-489, 2011
7. K.R. Foster, A. Lozano-Nieto, and P. Riu, “Heating of tissues by microwaves: a model analysis”, Bioelectromagnetics, 19, 420-428, 1998
8. K.R. Foster, H. N. Kritikos, H.P. Schwan, “Effect of surface cooling and blood flow on the microwave heating of tissue”, IEEE Trans Biomed Eng, 25, 313-316, 1978
9. Cazares, S.M., Snyder, J.A., Belanich, J., Biddle, J.C., Buytendyk, A.M., Teng, S.H.M. and O’Connor, K, “Active Denial Technology Computational Human Effects End-To-End Hypermodel for Effectiveness (ADT CHEETEH-E)”, Institute for Defense Analyses. IDA Document NS D-10435
10. Wang, H., Burgei, W. and Zhou, H., “A concise model and analysis for heat-induced withdrawal reflex caused by millimeter wave radiation”, American Journal of Operations Research, in press